Journal of Materials Chemistry B

Simulation-directed amplifiable nanoparticle enhanced quantitative scattering assay under low magnification dark field microscope

Journal:	*Journal of Materials Chemistry B*
Manuscript ID	TB-ART-02-2020-000350.R2
Article Type:	Communication
Date Submitted by the Author:	19-May-2020
Complete List of Authors:	Sun, Dali; North Dakota State University, Department of Electrical and Computer Engineering Yang, Li; Tulane University Lyon, Christopher; Tulane University Hu, Tony; Tulane University

COMMUNICATION

Simulation-directed amplifiable nanoparticle enhanced quantitative scattering assay under low magnification dark field microscopy

Received 00th January 2020,
Accepted 00th January 2020

DOI: 10.1039/x0xx00000x

Dali Sun [a], Li Yang [b], Christopher J Lyon [b], Tony Hu [b*]

Nanoparticle-enhanced assays read by high-magnification dark-field microscopy require time-intensive analysis methods subject to selection bias, which can be resolved by using low magnification dark-field assays (LMDFA), at the cost of reduced sensitivity. We have simulated and experimentally validated a tunable linker-based signal amplification strategy yielding 6-fold enhanced LMDFA sensitivity.

Gold nanoparticles are now in relatively widespread use for a variety of applications due to several useful physicochemical properties. Substantial effort has also been devoted to developing gold nanoparticle-based biosensors for noninvasive and targeted tumor diagnosis and treatment[1–6], but there are no widespread clinical applications for such approaches due to a trade-off between sensitivity and usability. We have previously described an automated low magnification dark-field assay (LMDFA) that reduces operator time and eliminates the selection bias associated with high magnification nanoparticle detection assays[7,8]. However, LMDFA has a different set of issues, including a greater susceptibility to signal artifacts, which can contribute to the reduced analytical sensitivity of this assay. LMDFA captures the signal of the entire assay well, but this means that nonspecific signals arising from sample contaminants or surface imperfections are also captured and can, therefore, cause artifacts that lower the signal-to-noise ratio (SNR) of the assay. LMDFA signal artifact effects can be attenuated through the use of an image processing algorithm[7], but this process can reduce assay sensitivity, and new approaches are needed to improve LMDFA sensitivity.

In this study, we report the development of a linker-based signal amplification approach that can be employed to increase the sensitivity of LMDFA detection. Nanoparticles created using noble metals can enhance scattering by surface plasmon resonance[9] and a pair of such closely spaced nanoparticle can produce "dimer" plasmons that can further enhance the scattering effect[10]. Simulations performed to determine optimal space between proximity nanoparticles were validated by experimental approaches, which determined that linker-based signal amplification could produce a six-fold increase in LMDFA signal, while retaining all the that advantages of a standard LMDFA, enhancing its potential for translation to clinical applications.

Theoretical modeling and simulation for amplification. Light scattered from AuNRs is subject to plasmonic enhancement when the distance between two or more AuNRs falls below the threshold for the formation of a local plasmon effect. In LMDFA, this distance is determined by the distance between two or more target molecules, and thus depends upon their relative expression on a target cell or vesicle or their surface accumulation upon capture from a sample of interest. The plasmonic effect used in LMDFA should, however, be capable of direct enhancement by linking other AuNRs to an AuNR already bound to the target protein, cell or vesicle to amplify this specific signal (Figure 1a). The linker approach adds two extra binding steps to the existing LMDFA approach: one to bind the linker to an AuNR already bound to a target immobilized on the detection well surface and a second to bind additional AuNRs to the first AuNR through its conjugated linkers. The length of the linkers used in this approach is critical to control the distance between the AuNRs in these assemblies and thus nanoplasmon formation and signal enhancement.

Finite-difference time-domain (FDTD), Mie approximation (T-Matrix), and finite element method (FEM) analyses are the most common methods used to compute the scattering of electromagnetic radiation by metallic nanoparticles[11]. FDTD calculates field vector components in a given instant in time, and Fourier transfer near-field solution to the frequency domain and propagated into the far-field by surface or volume integration. FDTD simulation confirmed the scattering enhancement of proximity nanoparticles (Supporting Information, Figure S1), but could not be used to conduct large-scale simulations due to the computing demands required to handle the complexity of such calculations. Mie approximation (T-Matrix) significantly simplifies the solution of the Maxwell equations by considering the scattering of light arisen from spherical objects. However, while it is possible to approximate the scattering from ellipsoid objects[12], this is not suitable for nanorods with complex spatial configurations. FEM solves the scattering problem by discretizing the Helmholtz equation to balance the computational complexity and is suitable for large-scale AuNR simulations.

Because the LMDFA analyzes the scattering of light from AuNR, which peaks at 650 nm, the FEM simulation was performed using a 650 nm incident light source, modeling variable distances between two AuNRs (25 × 60 nm). PEG was not included in the simulation since it does not deleteriously

[a] Department of Electrical and Computer Engineering, North Dakota State University, 1411 Centennial Blvd., 1015 Fargo, ND 58102.
[b] Department of Biochemistry and Molecular biology, Tulane University School of Medicine, New Orleans, LA 70112.
Electronic Supplementary Information (ESI) available: [details of any supplementary information available should be included here]. See DOI: 10.1039/x0xx00000x

affect AuNR or AgNR scattering at 650nm[13–15]. Scattering intensity at the center of these two particles (Figure 1b) was maximized when they were separated by 30 nm (Figure 1c). In agreement with FDTD simulation results, FEM simulation (Figure 1c) revealed that AuNR proximity caused maximized plasmonic scattering enhancement without a spectral aggregation shift[16] when the distance-to-diameter was ≈ 1.2. Since the LMDFA uses a halogen lamp with a 200 to 800 nm emission spectrum, scattering intensity produced by different AuNR separations was measured across this illumination spectra (Figure 1d). The sum of the scattering intensity from all wavelengths was then used to evaluate scattering enhancement under halogen illumination, which reached a maximum when AuNRs were separated by 40 nm (Figure 1e), confirming the optimal spacer distance required to maximize scattering intensity without spectral shift was similar when using halogen illumination. Simulations of both single wavelength and broad-spectrum illuminations indicated that there were marked declines in scattering intensity when particle separations exceeded 50 nm, and defined the maximum separation between the primary and secondary AuNRs for our amplification approach. Based on this observation, 2000 Da biotinylated PEG polymers (~20 nm long) were analyzed for their ability to amplify LMDFA signal in conjunction with streptavidin-conjugated AuNR.

To analyze how LMDFA signal should increase with particle abundance, a scaled-up simulation was constructed to mimic the accumulation of AuNRs on the LMDFA slide (Figure 1f). In this simulation, AuNRs were illuminated with a 200-800 nm light source positioned below the slide, and the scattered signal was detected at an angle perpendicular to the slide surface. Scattering intensity linearly correlated with the number of particles on the slide (Figure 1g), supporting the rationale for linking secondary particles to the biomarker probe to produce signal amplification.

Linker selection for signal amplification. Three different linker approaches were analyzed for their ability to connect AuNR particles to maximize scattering intensity: the binding between an avidin-conjugated AuNR and a biotinylated AuNR (Figure 2a) and between AuNR-AV particles linked by PEG400 and PEG2000 polymers biotinylated at their termini (Figure 2c). The absorbance spectra of AuNR samples were analyzed in the presence and absence of AuNR aggregation as a surrogate for enhanced scattering, since the Mie theory indicates that nanoparticle scattering intensity negatively correlates with the absorbance of the nanoparticle sample[17]. The first linking strategy involves streptavidin- and biotin-modified AuNR to form the "dimer". Mixtures of AuNR-AV and AuNR particles exhibited reduced absorbance relative to either nanoparticle alone (Figure 2b), but this effect produced only a modest increase (1.15-fold) in AuNR scattering. Incubation of AuNR-AV with bis-biotin functionalized PEG2000 (Biotin-PEG2000-Biotin), however, produced a marked decrease in AuNR absorption (Figure 2d) corresponding to an increase in AuNR scattering. Nonsignificant absorption changes (Figure 2d) observed upon mixing AuNR-AV and PEG2000, indicated an AuNR dimerization requirement for this change, and that PEG did not promote non-specific AuNR interaction or directly reduce sample absorption.

AuNR particles were next incubated with dilutions of biotinylated PEG400 and PEG2000 to analyze the effect of polymer length and concentration on AuNR-AV absorbance. Both PEG polymer lengths decreased AuNR absorbance in a concentration-dependent manner with good linear correlation (Figure 2e-h), but PEG2000 exhibited a better dynamic response (slope of -0.34 vs -0.18) than PEG400, where reduced absorption reflects enhanced scattering according to Mie theory. The greater absorption change observed in experiments using PEG2000 versus PEG400 as the linker may be explained by nearest neighbor interactions due to the rapid decay of electronic overlap between bands in adjacent nanoparticles, as proposed by Remacle *et al*[18]. This observation can also be explained by the scattering simulation result shown in Figure 1c and e. According to Mie theory, absorption, extinction, and scattering coefficient changes produced upon linker addition should follow $\Delta\sigma_{abs} = \Delta\sigma_{ext} - \Delta\sigma_{sca}$. AuNR interactions mediated via the PEG400 linker should exhibit a <20nm spacing, resulting in lower AuNR scattering, and thus lower absorption than PEG2000 linkers.

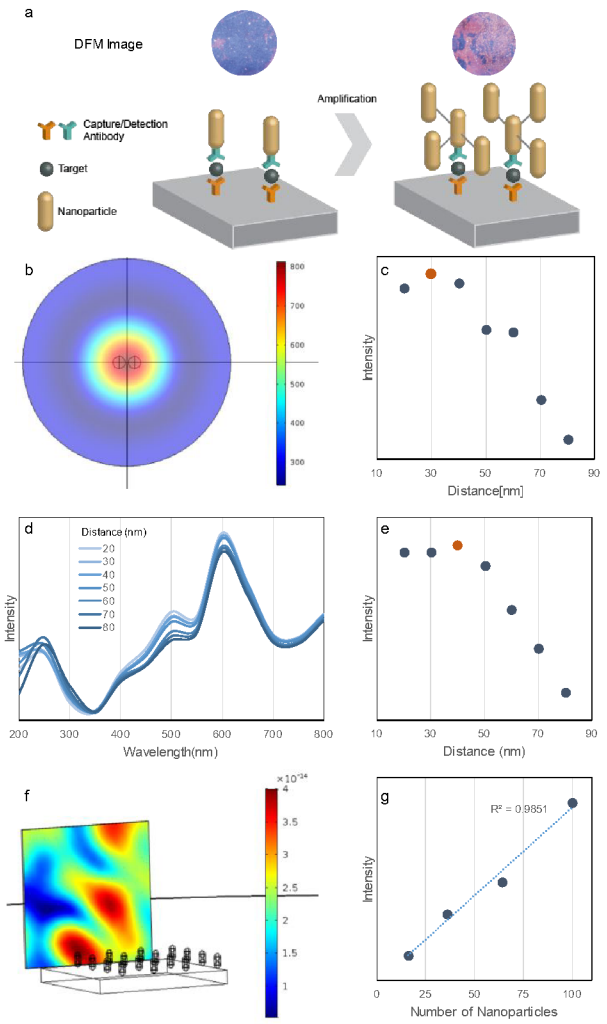

Figure 1. Modeling and simulation. a) LMDFA amplification scheme. Simulated b) heat map and c) intensity plot of scattering intensity versus distance between AuNR pairs with 650nm incident light source. Graph of d) the scattering intensity spectrum and e) its summed intensity versus distance between AuNR pairs under broad spectrum (200-800 nm) illumination. Simulation of the scattering signal generated under 200-800 nm illumination showing the f) scatter distribution from an AuNR array (see Figure S2 for details) and g) scatter intensity versus AuNR number in this the array.

Signal amplification in LMDFA. The above simulations and experiments suggested a feasible linker-based amplification strategy. To apply this scheme to an LMDFA, we employed a

multi-step approach (Figure 3ab) where primary AuNR-AVs bound to the biotinylated antibody immobilized on the assay well surface, as a surrogate to a target biomarker. These AuNR-AVs were then incubated with bis-biotin labeled PEG linkers and then hybridized with AuNR-AVs to induce AuNR dimerization. This approach resulted in 6-fold LMDFA signal amplification versus that detected from wells incubated with primary AuNR-AVs alone (Figure 3c). Analysis of a serial dilution of surface-bound primary AuNR-AV particles that were evaluated as a surrogate for a biomarker dilution (Figure 3d), found that linker-medidated AuNR-AV dimerization increased LMDFA signal detected at low AuNR-AV concentrations to distinguish samples that did not differ when analyzed without secondary AuNR-AV addition.

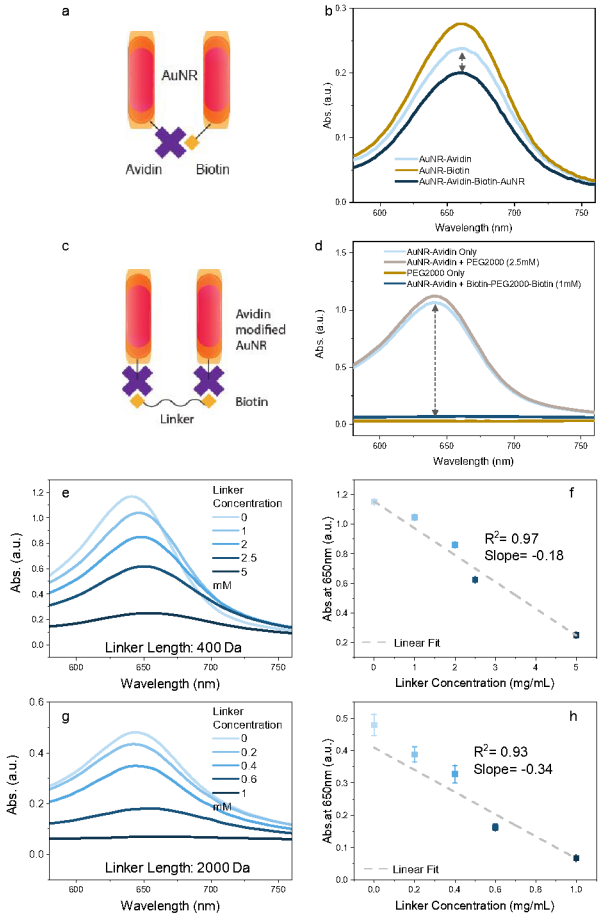

Figure 2. a,b) AuNR avidin-biotin signal amplification schemes and UV-IR absorption spectrum of the unlinked and linked AuNR particles. c,d) AuNR-AV PEG-biotin signal amplification scheme and UV-IR absorption spectra. e,g) UV-IR absorption spectra and f,h) 650 nm scattering intensity detected with AuNR-AV mixed with bis-biotin PEG400 and PEG2000 linker dilutions, respectively. Data points represent mean ± SE, n = 4.

These results indicate that this approach can improve the LMDFA detection limit. Normalization of the LDMFA signal in the low concentration samples to the background sample (Figure 3e) revealed that this linker amplification approach also significantly increased the slope of LDMFA signal in response to concentration (0.17 vs 0.03) without affecting variability (R^2; 0.82 vs 0.77), suggesting that amplification can improve the sensitivity of LMDFA for more precise quantitation of low concentration samples.

Conclusions

We have previously described an automated LMDFA approach that can detect exosomes derived from malignant or infected cells in serum samples for pancreatic cancer and TB screening[7,8].

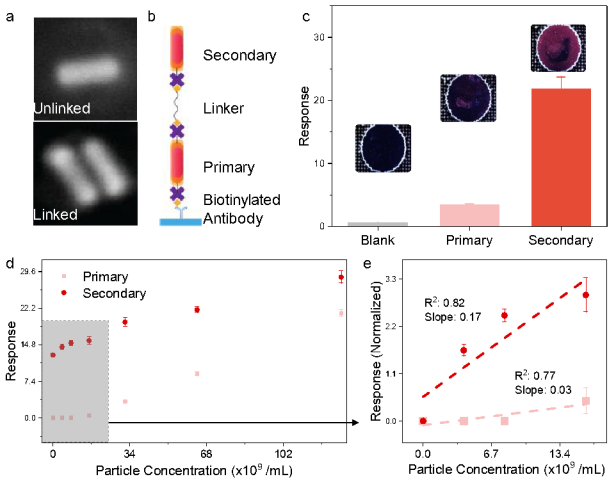

Figure 3 a) SEM images of unlinked and linked AuNR. b,c) LMDFA amplification scheme and comparison of signal from single and dimerized AuNR-AVs. d) LMDFA response from serially diluted primary AuNR-AVs bound to the surface of the assay well with or without hybridization to a fixed concentration of secondary AuNR-AVs after incubation with bis-biotin PEG2000 linker, where the response at low primary AuNR-AV concentration (small boxed region) is background-normalized and regraphed to e). Data points represent mean ± SE, n = 4.

The use of LMDFA in these studies solved critical issues for clinical translation of nanoparticle-based assays, by reducing the operational complexity and bias associated with quantification of nanoparticle signal by high magnification image analysis, at the cost of reduced sensitivity.

Results of this study confirm our simulation-based hypothesis the sensitivity of LMDFAs can be enhanced by a linker-mediated approach to amplify the nanoplasmonic signal from nanoparticle probes bound to the assay target. While further refinements may be possible to further improve the sensitivity and throughput of LMDFAs, this study offers proof-of-principle data that this linker-based amplification strategy can extend LMDFA sensitivity. Moreover, the streamlined nature of this assay and its readout suggest that such LMDFAs could be of useful in both research and clinical settings.

Acknowledgment

The authors gratefully acknowledge funding from the Eunice Kennedy Shriver Institute of Child Health & Development of the National Institutes of Health (R01HD090927); National Institute of Allergy and Infectious Diseases of the National Institutes of Health (R01AI122932 and R21AI126361); National Institute of Biomedical Imaging and Bioengineering of the National Institutes of Health (R21EB026347); U.S. Department of Defense (W8IXWH1910926).

References

1 S. Jain, D. G. Hirst and J. M. O'Sullivan, *Br. J. Radiol.*, 2012, **85**, 101–113.
2 C. L. Ventola, *P T*, 2017, **42**, 742–755.
3 E. C. Dreaden, A. M. Alkilany, X. Huang, C. J. Murphy and M. A. El-Sayed, *Chem. Soc. Rev.*, 2012, **41**, 2740–2779.
4 S. D. Brown, P. Nativo, J.-A. Smith, D. Stirling, P. R. Edwards, B. Venugopal, D. J. Flint, J. A. Plumb, D. Graham and N. J. Wheate, *J. Am. Chem. Soc.*, 2010, **132**, 4678–4684.
5 C. H. J. Choi, C. A. Alabi, P. Webster and M. E. Davis, *Proc. Natl. Acad. Sci.*, 2010, **107**, 1235–1240.
6 K. Liang, F. Liu, J. Fan, D. Sun, C. Liu, C. J. Lyon, D. W. Bernard, Y. Li, K. Yokoi, M. H. Katz, E. J. Koay, Z. Zhao and Y. Hu, *Nat. Biomed. Eng.*, 2017, **1**, 1–16.
7 D. Sun, J. Fan, C. Liu, Y. Liu, Y. Bu, C. J. Lyon and Y. Hu, *Anal. Chem.*, 2016, **88**, 12001–12005.
8 D. Sun and T. Y. Hu, *Biosens. Bioelectron.*, 2018, **99**, 513–518.
9 S. Eustis and M. A. El-Sayed, *Chem. Soc. Rev.*, 2006, **35**, 209–217.
10 C. E. Talley, J. B. Jackson, C. Oubre, N. K. Grady, C. W. Hollars, S. M. Lane, T. R. Huser, P. Nordlander and N. J. Halas, *Nano Lett.*, 2005, **5**, 1569–1574.
11 J. Parsons, C. P. Burrows, J. R. Sambles and W. L. Barnes, *A comparison of techniques used to simulate the scattering of electromagnetic radiation by metallic nanostructures*, 2010, vol. 57.
12 M. Quinten, *Optical Properties of Nanoparticle Systems*, Wiley-VCH Verlag GmbH & Co. KGaA, Weinheim, Germany, 2011.
13 P. Šimáková, J. Gautier, M. Procházka, K. Hervé-Aubert and I. Chourpa, *J. Phys. Chem. C*, 2014, **118**, 7690–7697.
14 T. Niidome, M. Yamagata, Y. Okamoto, Y. Akiyama, H. Takahashi, T. Kawano, Y. Katayama and Y. Niidome, *J. Control. Release*, 2006, **114**, 343–347.
15 G. Zhang, Z. Yang, W. Lu, R. Zhang, Q. Huang, M. Tian, L. Li, D. Liang and C. Li, *Biomaterials*, 2009, **30**, 1928–1936.
16 I. E. Sendroiu, S. F. L. Mertens and D. J. Schiffrin, *Phys. Chem. Chem. Phys.*, 2006, **8**, 1430–1436.
17 P. K. Jain, K. S. Lee, I. H. El-sayed and M. A. El-sayed, 2006, 7238–7248.
18 G. Markovich, C. P. Collier, S. E. Henrichs, F. Remacle, R. D. Levine and J. R. Heath, *Acc. Chem. Res.*, 1999, 32, 415–423.

